J. Fluid Mech. (1984), *vol.* 140, *pp.* 27–44
Printed in Great Britain

Turbulent flow over large-amplitude wavy surfaces

By JEFFREY BUCKLES, THOMAS J. HANRATTY
Department of Chemical Engineering, University of Illinois, Urbana, 61801

AND RONALD J. ADRIAN
Department of Theoretical and Applied Mechanics, University of Illinois, Urbana, 61801

(Received 12 May 1983 and in revised form 17 October 1983)

The laser-Doppler velocimeter is used to measure the mean and the fluctuating velocity for turbulent flow over a solid sinusoidal wave surface having a wavelength λ of 50.8 mm and a wave amplitude of 5.08 mm. For this flow, a large separated region exists, extending from $x/\lambda = 0.14$ to 0.69. From the mean velocity measurements, the time-averaged streamlines and therefore the extent of the separated region are calculated. Three flow elements are identified: the separated region, an attached boundary layer, and a free shear layer formed by the detachment of the boundary layer from the wave surface. The characteristics of these flow elements are discussed in terms of the properties of the mean and fluctuating velocity fields.

1. Introduction

Fluid flowing over a wavy surface experiences large positive and negative pressure gradients because of the wave-induced expansion and contraction of the streamlines.

At the wave surface these pressure gradients are balanced by viscous effects represented by the term $\mu\,\partial^2 U/\partial y^2$ in the momentum equation. Consequently regions of unfavourable pressure gradient behind the wave are accompanied by positive values of $\partial^2 U/\partial y^2$ at $y = 0$ and therefore inflexional profiles. For large enough wave amplitudes the unfavourable pressure gradients are sufficient to cause separation.

Considerable progress has been made in recent years in presenting solutions for turbulent flow over small-amplitude waves for which a separated region does not exist (Thorsness, Morrisroe & Hanratty 1978; Zilker, Cook & Hanratty 1977). However, adequate descriptions are not available for flow over large-amplitude waves. A computational method for analysing laminar flows has recently been presented by Caponi *et al.* (1982). The chief theoretical problem in extending this method to turbulent flows is the specification of the Reynolds stresses. The solution of this problem appears more difficult for large- than for small-amplitude waves because of uncertainties in dealing with the separated region. Consequently, there is a need for information about the extent of this region and the details of the flow within it.

Zilker & Hanratty (1979) presented a review of experimental studies of flow over large-amplitude waves. These give results on the pressure and shear-stress variation along a wave surface but little reliable quantitative results about the separated region. In an effort to obtain such information, Zilker & Hanratty used electrochemical probes to measure the wall shear stress, thermal split-film probes to measure the velocity and visual techniques to display flow patterns. These experiments gave an approximate indication of the extent of the separated region but were not adequate for providing proper guidance for modelling the turbulence. The chief difficulty is that

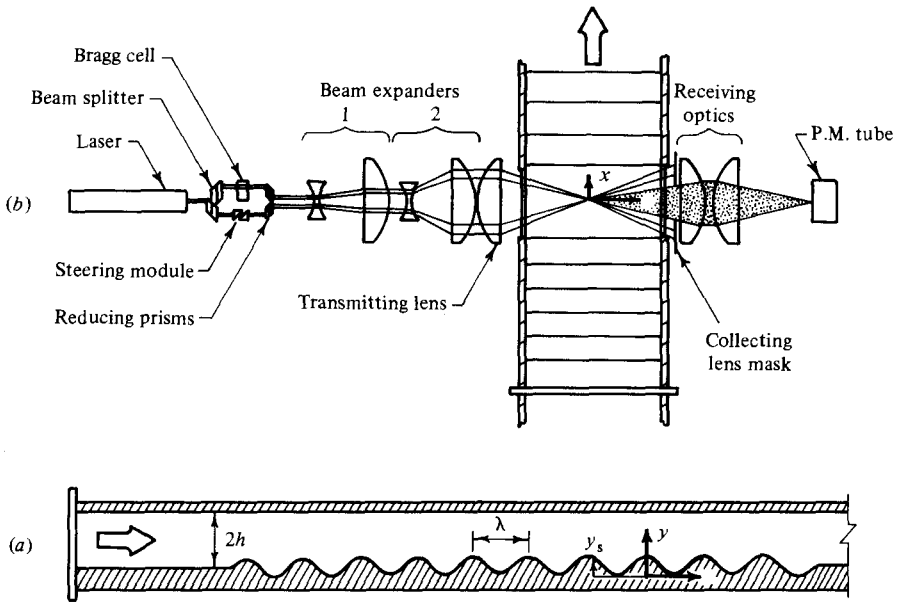

FIGURE 1. LDV system layout (*a*) and test section (*b*).

a turbulent separated region is highly disturbed, the flow fluctuations being considerably larger than the mean flow. Classical techniques, such as hot-film probes, cannot measure the velocity in such situations. Consequently, a number of recent studies of turbulent separated flows (Simpson, Strickland & Barr 1977; Durst & Pereira 1982; Etheridge & Kemp 1978; Simpson, Chew & Shivaprasad 1981*a*, *b*) have used the laser-Doppler velocimeter because it provides an unobtrusive technique that measures the instantaneous velocities of neutrally buoyant particles. This paper describes experiments that used this technique to study the flow over large-amplitude waves.

The experiments were carried out in the horizontal rectangular water channel used by Zilker & Hanratty (1979). Tests were conducted over the eighth wave in a series of ten waves that were located on the bottom wall of the channel on its downstream end. The channel was long enough that a fully developed turbulent flow was obtained at the beginning of the wavetrain, and wide enough that the mean flow was essentially two-dimensional. Measurements were made of the mean velocity U in the streamwise direction and the pressure along the surface of the wave. The wavelength was $\lambda = 50.8$ mm and the wave amplitude was $a = 5.08$ mm (one-half of the peak-to-trough distance), with ratio $2a/\lambda = 0.20$. The bulk velocity, defined as the average of the mean velocity across the channel, was $U_b = 51$ cm s^{-1}, and the Reynolds number based on U_b and the half-height h of the channel was $Re = 12000$.

2. Experimental apparatus and procedure

The Plexiglas test section in which the measurements were performed was 1.47 m long with a rectangular cross section $2h = 47.4$ mm high and 610 mm wide. The top of the channel was flat. Sinusoidal waves were machined in the bottom with the mean wave level at the level of the smooth lower wall, as shown in figure 1 (*a*), so that there was no change in the mean cross-sectional area. The test section was preceded by 7.16 m of rectangular channel which provided approximately 70 hydraulic diameters

for flow development. The existence of fully developed turbulent flow at the entrance to the test section has been verified by Zilker (1976) and by Thorness (1975).

Measurements of the streamwise component (x-direction) of velocity in the water flow were made using a single-channel dual-beam laser-Doppler velocimeter operated in forward-scatter mode (figure 1*b*). The LDV consisted of a 15 mW Spectra-Physics He–Ne laser and TSI optics and photomultiplier tube. A traverse mechanism provided 0.025 mm resolution in the y-direction and motion in the x-direction.

Two 2.27:1 beam expansion units (TSI, Inc., Model 9188) were used in series to reduce the measurement volume dimensions and to provide high signal-to-noise ratio by increasing the illuminating beam intensity in the measurement volume. With a 250 mm focal-length transmitting lens, the measurement volume, defined by the e^{-2} intensity distribution of the illuminating beams, was an ellipsoid with dimensions 0.035, 0.035 and 0.38 mm in the x-, y- and z-directions. The measurement volume was located within 25 mm of the midspan of the channel. The optical axes of the transmitting optics and the receiving optics were each inclined downards at 5° angles to permit clear optical access to all regions of the wave trough. Since the receiving optics viewed the measurement volume at a net 10° angle, its length in the spanwise direction was slightly smaller than the value indicated above (0.38 mm); however, the spatial resolution in the y-direction was increased to 0.07 mm approximately, because the ellipsoid tilted downwards. The y-location of the measurement volume with respect to the surface of the wave was determined to within an estimated accuracy of ± 0.07 mm by approaching the surface until the incident illuminating beams and their reflections were symmetric to visual inspection. Reliable measurements could be made at locations as close as 0.13 mm to the surface, but below this value the signals became too noisy for accurate measurement, and the signal processor would intermittently lock onto the zero-velocity frequency corresponding to scattering from the wall.

The Doppler signals were frequency-shifted by 200 kHz to permit measurement of negative velocities, and high-pass filtered at 100 kHz to remove the pedestal components prior to processing. The processor was a TSI, Model 1090, frequency tracker operated on its 500 kHz range. The tracker held its output voltage at the last known value during the Doppler-signal dropout. Early measurements were made with natural particles serving as scatterers, but the best results were obtained by filtering the water to remove particles larger than 5 μm and adding 0.5 μm latex spheres (Dow Chemical) in amounts sufficient to produce approximately one processable particle in the measurement volume, on average. Under these conditions, data rates of 2000–4000 samples per second were achieved at a flow rate of 0.4 m s^{-1}. The resulting signals from the tracker had 'high data density' (Adrian 1983); i.e. there were many velocity samples per Taylor miscroscale of the flow. In this regime of operation, the step changes that occur in the output of the tracker at each velocity update are small in amplitude, and low-pass filtering the signal to smooth the steps yields an accurate representation of the original, continuous velocity signal. Consequently, after low-pass filtering the output voltage of the tracker at 1 kHz, an approximately continuous signal was obtained. This signal was subsequently sampled at 80 Hz by an 8-bit A/D converter. Digital analysis of these data used ordinary algorithms for uniformly sampled data; i.e. corrections for LDV velocity biasing were not necessary.

The accuracy of the mean-velocity measurement was evaluated in several ways. Mean-velocity estimates were typically calculated by averaging batches of either 1000 samples in the upper half of the channel or 4000 samples in the lower half. The

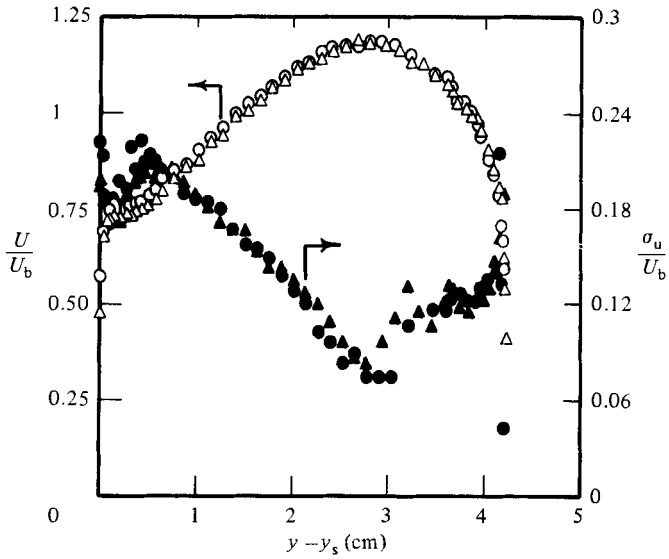

FIGURE 2. Flow periodicity. U/U_b; ○, $x/\lambda = 0$; △, $x/\lambda = 1.0$. σ_u/U_b; ●, $x/\lambda = 0$; ▲, $x/\lambda = 1.0$.

corresponding root-mean-square uncertainties in the means were estimated to be 0.2 and 0.5% respectively at the points of largest turbulence intensity in each region. Tests conducted with two smooth walls yielded mean-velocity profiles whose logarithmic regions were fitted with 2% accuracy by a log law with a von Kármán constant equal to 0.41 and an additive constant equal to 5.5, in agreement with published measurements using other techniques. Reproducibility was checked by integrating the mean velocity profiles to obtain the volume flow rates at various streamwise locations. Typically, these flow rates agreed to within 0.5%. The ratio of centreline velocity to bulk velocity obtained at Reynolds number 12000 was 1.2 ± 0.05, in good agreement with the data in the literature.

Noise in the measurements of velocity was attributed to noise in the signals from the LDV photodetector, noise in the signal-processing electronics, and phase or ambiguity noise caused by occasional random overlapping of particles in the measurement volume. The power spectrum of the noise was determined experimentally to be white up to the maximum frequency that was studied (3 kHz). Hence George's (1974) method of extrapolating the noise spectrum to zero frequency was used to obtain an estimate of the variance of the noise. Under the assumption that the noise was statistically independent of the velocity signal, measurements of the variance of the velocity were corrected by subtracting the variance of the noise. This resulted in a maximum correction to the root-mean-square velocity that was less than 3.5% of the root mean square. Corrections to higher-order moments such as skewness and flatness were not made because of the small magnitude of the noise contribution. The measured value of the root-mean-square streamwise velocity fluctuation in the channel flow experiment with two smooth walls at Reynolds number 12000 was 0.05 of the maximum velocity. For comparison, Reischman & Tiederman (1975) obtained 0.04 at Reynolds number 14360 and 0.048 at Reynolds number 6430.

Measurements were performed over the eighth wave downstream from the entrance to the test section. The periodicity of the flow over this cycle of the wavetrain is demonstrated by comparison of the profiles of mean velocity and turbulence intensity

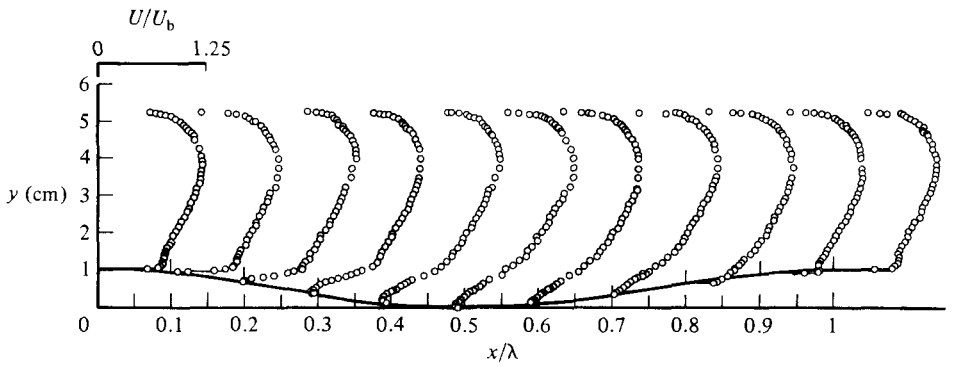

FIGURE 3. Mean-velocity profile sequence.

measured at the start of the wave, $x = 0$, and the end, $x = 50.8$ mm (figure 2). The mean velocities repeat to within 1 % experimental accuracy, except near the wave surface, where there is approximately 5 % flow retardation over one wavelength. The turbulence intensity reveals a somewhat less perfect approach to periodicity especially near the wall.

Measurements of mean pressure and root-mean-square pressure fluctuations were obtained at 33 locations using 1.59 mm vertical parallel surface taps spaced at 1.59 mm intervals in the streamwise direction along the surface of the eighth wave. Pressures were measured with a C. J. Enterprises differential pressure cell and carrier modulator having 10 V/in. H_2O sensitivity and 1 ms time constant, and pressure data were digitized at 80 Hz rates.

3. Experimental results

3.1. *Separated-flow region*

All experimental results will be presented in terms of y, the distance above the trough of the eighth wave, and x, the distance downstream of its crest (cf. figure 1 (*a*). The position of the wave surface is given by

$$y_s = a + a\cos\frac{2\pi x}{\lambda}, \tag{1}$$

and the bulk velocity, evaluated at any location x, is given by

$$U_b = [2h + a - y_s(x)]^{-1} \int_{y_s(x)}^{2h+a} U(x, y)\,dy. \tag{2}$$

Mean-velocity profiles at different values of x/λ are shown in figure 3. The first point in each profile was measured at a distance of 0.13 mm above the wave surface. The profiles indicate flow separation between $x/\lambda = 0.1$ and $x/\lambda = 0.2$, where the mean direction of flow measured nearest the wall reverses from a positive value to a very slightly negative value. Similarly, reattachment occurs between $0.6 \leqslant x/\lambda \leqslant 0.7$, where the velocity measured nearest the wall returns to a positive value. In order to locate the points of separation and reattachment better, we have plotted the velocity at 0.13 mm above the wave surface versus downstream distance and interpolated to obtain the downstream locations at which this velocity changes signs. If the velocity were a linear function of position between the lowest points on each profile and the wave surface, this procedure would amount to interpolating for the points of vanishing wall shear stress. This plot, which also used mean-velocity data

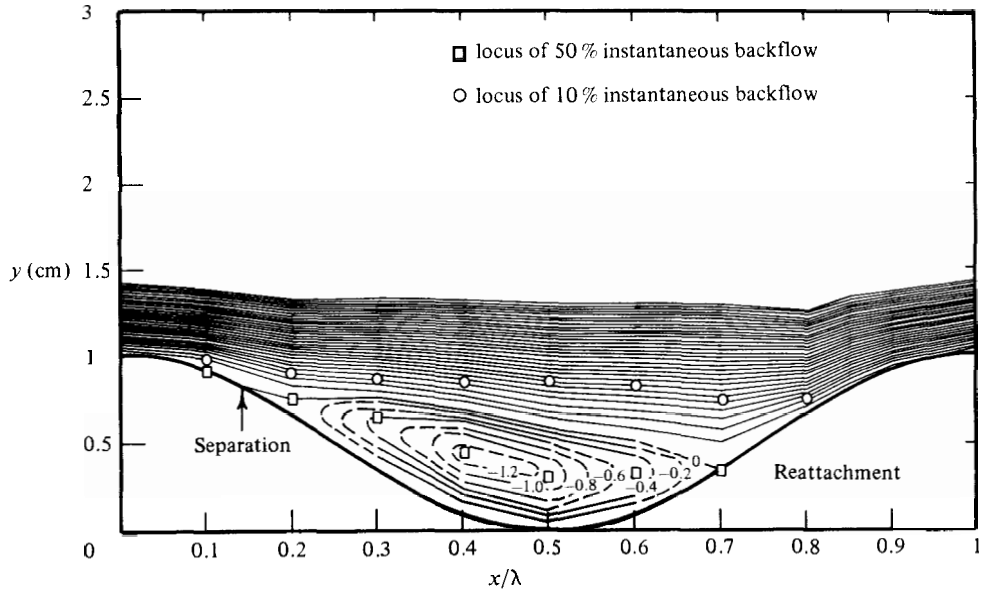

FIGURE 4. Streamline map.

at $x/\lambda = 0.15$, 0.75 and 0.85 not shown on figure 3, indicates that separation occurs at $x/\lambda = 0.14$ and that reattachment occurs at $x/\lambda = 0.69$. These values compare favourably with the separation and reattachment locations of 0.08 and 0.70 at Reynolds number 15600 and 0.1 and 0.65 at Reynolds number 8300 inferred by Zilker & Hanratty (1979) for $2a/\lambda = 0.2$, from observation of dye streaks.

The stream function for the mean flow has been calculated by integrating the mean-velocity profiles,

$$\Psi(x, y) = \int_{y_s}^{y} U(x, y')\,\mathrm{d}y', \tag{3}$$

and the resulting streamlines are shown in figure 4. Streamlines lying above the $\Psi = 0$ streamline are plotted at increments of $\Delta\Psi = 5$, and those lying in the recirculating region are plotted at increments of 0.2. Dashed lines indicate portions of the streamlines that were obtained by interpolation.

The $\Psi = 0$ streamline necessarily begins at $x/\lambda = 0.14$ and ends at $x/\lambda = 0.69$ because these are points where Ψ has been found to vanish at the surface. Between these points the recirculating zone reaches a maximum thickness of 6 mm at $x/\lambda = 0.4$, corresponding to approximately 60% of the peak-to-trough wave height. The $\Psi = 0$ streamline intersects the downstream surface of the wave at an angle approximately 40° from the normal to the surface, and the mean-flow pattern in the vicinity of reattachment is similar, in some regards, to a stagnation-point flow. Immediately above the separation point the flow appears to be deflected first up and then down. The split-film velocity data of Zilker & Hanratty (1979) suggest similar behaviour. Downstream of the reattachment point the flow streamlines are compressed upwards in response to the lifting wave surface, indicating a significantly accelerated flow.

The mean surface pressure along the wavetrain is a combination of a linearly decreasing trend plus a periodic variation. As shown in figure 5, the periodic variation is much greater than the channel pressure drop per wavelength for the present wave. Separation occurs in a region of adverse pressure gradient, which extends downstream

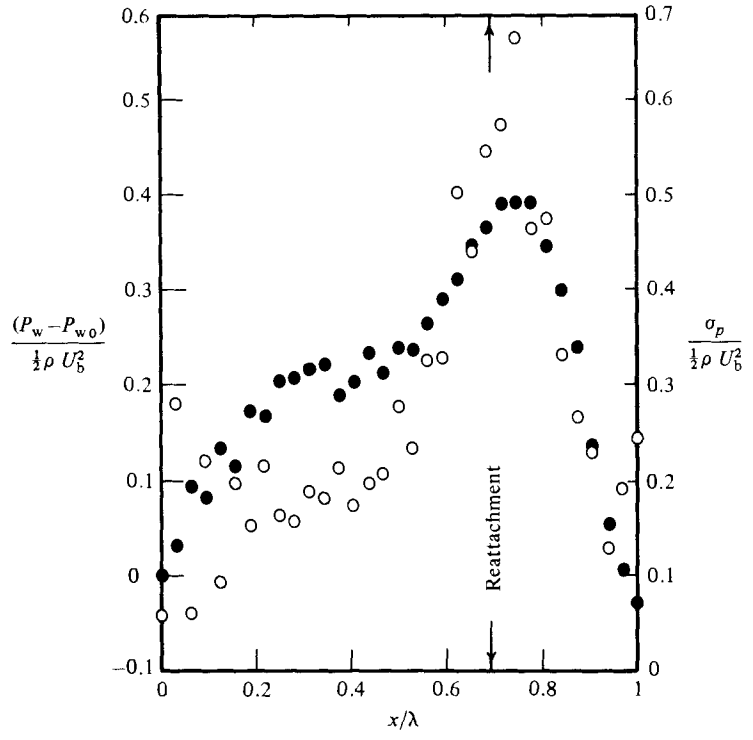

FIGURE 5. Time-averaged pressure distribution: ●, time-averaged pressure relative to upstream crest; ○, time-averaged root-mean-square pressure fluctuations.

to about $x/\lambda = 0.25$ and precedes a region where the pressure becomes nearly constant over the central portion of the separation bubble.

In the neighbourhood of reattachment the mean-pressure distribution on the surface is similar to that which would be produced by a stagnation-point flow with impingement at an oblique angle to the surface. However, the point of reattachment defined by vanishing mean wall shear stress occurs approximately 0.05λ ahead of the pressure maximum, whereas it would coincide with the pressure maximum in a steady stagnation-point flow. Mean-velocity profiles, to be presented shortly, suggest the formation of a thin, growing wall boundary layer originating at the point of reattachment and accelerating strongly downstream of reattachment. Thus one of the consequences of the delayed pressure maximum is strong boundary-layer acceleration in a nearly vanishing pressure gradient. Similar behaviour has been observed in the reattachment region of separated flows by Robertson *et al.* (1977), Hillier & Cherry (1982) and many others. The overall pressure distribution suggests that the wall boundary layers between $0 < x/\lambda < 0.25$ and $0.7 < x/\lambda < 1.0$ are strongly dependent on the outer field, whereas the separation bubble is driven by mechanisms other than an externally imposed pressure gradient.

Measurements of the root-mean-square value of the pressure fluctuations σ_p are also shown in figure 5. These are of large magnitude, being of the same order as the local mean-pressure difference. Comparison of the observed root-mean-square pressure coefficients $\sigma_p/\frac{1}{2}U_b^2$ with data from other separated flows is complicated because the velocity scales used in the definition of the pressure coefficients are not directly comparable. Even so, the root-mean-square pressure-coefficient data of Mabey (1972) and Robertson *et al.* (1977), defined using freestream velocity, are generally of the

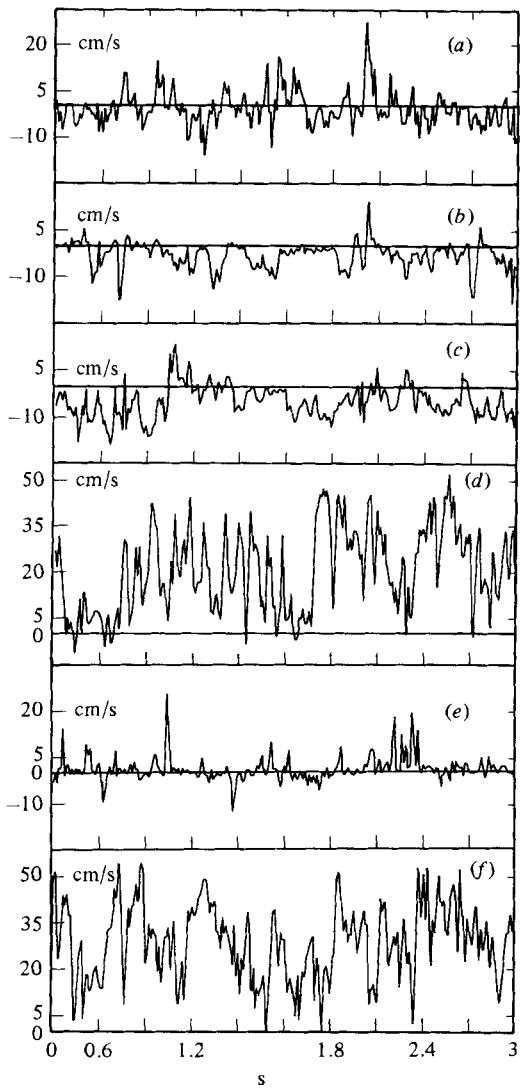

FIGURE 6. Velocity time traces:

	x/λ	$y-y_s$ (mm)	U/U_b	γ	σ_u/U_b	S	F
(*a*)	0.15	0.13	−0.008	0.49	0.11	0.61	7.5
(*b*)	0.30	0.13	−0.047	0.31	0.085	−0.31	5.2
(*c*)	0.30	1.02	−0.088	0.21	0.13	0.79	5.0
(*d*)	0.30	5.84	0.45	0.95	0.27	−0.0048	2.5
(*e*)	0.70	0.13	0.019	0.60	0.086	1.6	8.7
(*f*)	0.70	7.62	0.49	0.98	0.24	−0.19	2.6

same level as our data. Mabey's (1972) data show a trend toward lower values with increasing flow velocity. The most striking feature of the profile representing the variation of σ_p in the x-direction is the sharp maximum located downstream of the reattachment point and close to the point of maximum mean pressure. The value of σ_p at this maximum is too large to be explained entirely by wandering of the reattachment location. Rather, it appears to be influenced by wide variations of the velocity of the fluid impinging on the wall at reattachment. These unsteady motions

may be a combination of the unsteadiness caused by the passage of large-scale structures and by unsteadiness associated with the location of the reattachment point fluctuating upstream and downstream (Abbot & Kline 1962; Kim, Kline & Johnston 1978; Hillier & Cherry 1982).

Typical velocity histories measured at selected points in the flow are shown in figures 6(*a*, *f*). The 80 Hz sampling rate used to obtain the data from which the plots have been constructed was insufficient to resolve all of the scales of motion. However, we estimate that it was large enough to resolve energy-containing motions, so the histories reproduced in figure 6 are believed to be representative of the large-scale velocity fluctuations. In the caption for these figures we identify the local value of U/U_b and the variance σ_u, skewness factor S and the flatness factor F characterizing the distribution function for the fluctuations in velocity u:

$$\sigma_u = (\overline{u^2})^{\frac{1}{2}}, \tag{4}$$

$$S = \overline{u^3}/\sigma_u^3, \tag{5}$$

$$F = \overline{u^4}/\sigma_u^4. \tag{6}$$

Also given is the intermittency γ, defined as the fraction of time that u is positive. It is identical with the quantity γ_{pu} used by Simpson *et al.* (1981*a*, *b*).

The data at $x/\lambda = 0.15$ in figure 6(*a*) represent flow very near the point of separation and very close to the wall. The flow is equally positive and negative, and the skewness is small and positive, indicating a slight tendency towards dominant positive fluctuations. The flatness value of approximately 7.5 implies an intermittent process with equally strong positive and negative fluctuations. The amplitudes of these strong fluctuations are roughly twice the background amplitude.

Data obtained at $x/\lambda = 0.3$, presented in figures 6(*b–d*), are representative of flow in the middle of the separation bubble. Close to the wall the velocity exhibits substantial periods of inactivity when it remains close to zero, followed by large negative fluctuations (figure 6*b*). The mean velocity is slightly negative at this point, and the flow is reversed almost 70% of the time. When positive fluctuations occur, they are usually in the form of rapid spikes separated by a mean period of about 0.6 s. At the location of maximum reversed mean flow (figure 6*c*) the periods of zero velocity are shorter, and the periods of reversed flow are correspondingly longer. Reversed flow occurs approximately 80% of the time. At $y-y_s = 5.84$ mm (figure 6*d*) the y-profile of the fluctuation intensity shows a local maximum. As we shall see, this maximum is associated with the centreline of a shear layer that originates close to the point of separation. The mean velocity is $0.445U_b$, but, instantaneously, the velocity almost reaches $U_b = 50.7$ cm/s and occasionally drops below zero. The very large range of fluctuations must be considered when interpreting measurements made with instruments that require linearization about a mean operating value, such as thermal anemometers.

The flow close to the wall in the vicinity of reattachment is represented in figure 6(*e*). The mean velocity and the root mean square of the velocity fluctuations are both small, but the root mean square is approximately four times the mean. The flow is forward about 60% of the time, and it is characterized by generally small fluctuations interspersed with large positive spikes and significantly less frequent negative spikes. Directly above this point, at $y-y_s = 7.62$ mm (figure 6*f*), the flow is similar to the shear-layer behaviour observed in figure 6(*d*).

Profiles of the local intermittency at various downstream stations are shown in figure 7. The loci of the 10 and 50% intermittency points have been determined from

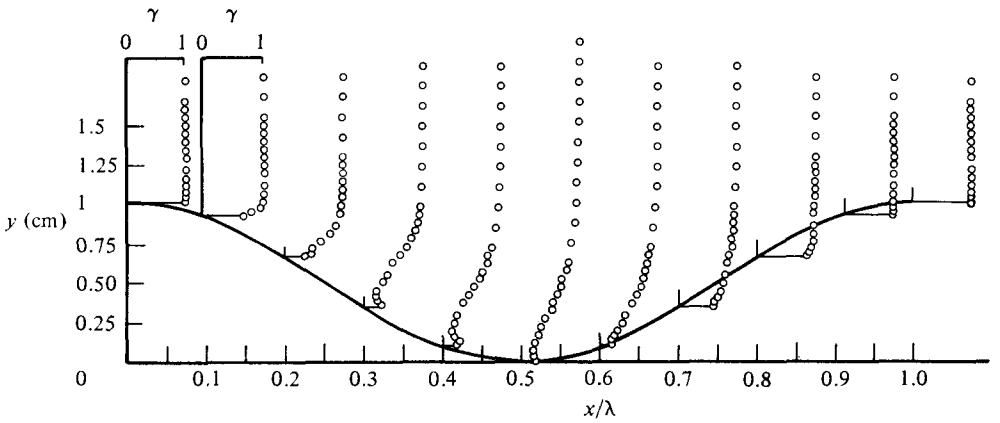

FIGURE 7. Flow intermittency.

those profiles and plotted on figure 4. The 50 % intermittency line originates very near the point of separation, at $x/\lambda = 0.14$, and terminates very near the point of reattachment. Between these locations the occurrence of 50 % intermittency is well correlated with the occurrence of zero mean streamwise velocity. For example, the locus of the 50 % line passes through the centre of the recirculating flow vortex shown in figure 4. The locus of 10 % intermittency resides surprisingly far above the wave surface. At $x/\lambda = 0.5$ the flow is reversed 10 % of the time at a distance above the $\psi = 0$ streamline that is almost one-half of the maximum thickness of the recirculating zone.

Figure 7 shows that flow reversals occur a significant fraction of the time near the surface at $x/\lambda = 0.1$, and similarly at $x/\lambda = 0.8$, fully 0.1λ downstream of the reattachment point. The prevalence of reversed-flow occurrences at these locations suggest that the flow must be unsteady to a significant degree at both reattachment and separation. The minimum value of the intermittency occurs at $x/\lambda = 0.4$ where the flow at the location of maximum mean reversed flow is in the reversed flow direction over 82 % of the time.

The intermittency profiles at $x/\lambda = 0.3$, 0.4, 0.5 and 0.6 each display regions of increased forward flow as the wall is approached. Similar behaviour was noted by Simpson *et al.* (1981*a*), who attributed it to wallward-moving fluid spreading outwards as it impacts the wall, thereby partially cancelling the reversed flow motion some of the time.

3.2. *Profiles of mean velocity*

Profiles of the mean velocity are shown in figure 8 for $x/\lambda = 0.7$, 0.75, 0.8, 0.9, 1.0 and 0.1, and in figure 9 for $x/\lambda = 0.15$, 0.2, 0.3, 0.4, 0.5 and 0.6. The coordinate $y - y_s$ represents the distance of above the wave surface.

The profiles at $x/\lambda = 1$, 0.1 clearly show a thin forward-moving boundary layer close to the wave surface. The sharp increase of the velocity at the point closest to the surface ($y - y_s = 0.13$ mm) from $x/\lambda = 0.7$ to $x/\lambda = 0.75$ indicates that the boundary layer is initiated approximately at the reattachment point ($x/\lambda = 0.69$). This boundary layer is quite thin, being less than 0.15 mm at $x/\lambda = 0.75$, 0.8 and about 0.6 mm at the wave crest, $x/\lambda = 0$. Beyond $x/\lambda = 0$ it becomes much thicker, approximately tripling in size from $x/\lambda = 0$ to the separation point. There is also a suggestion of a boundary layer moving a short distance upstream from the re-

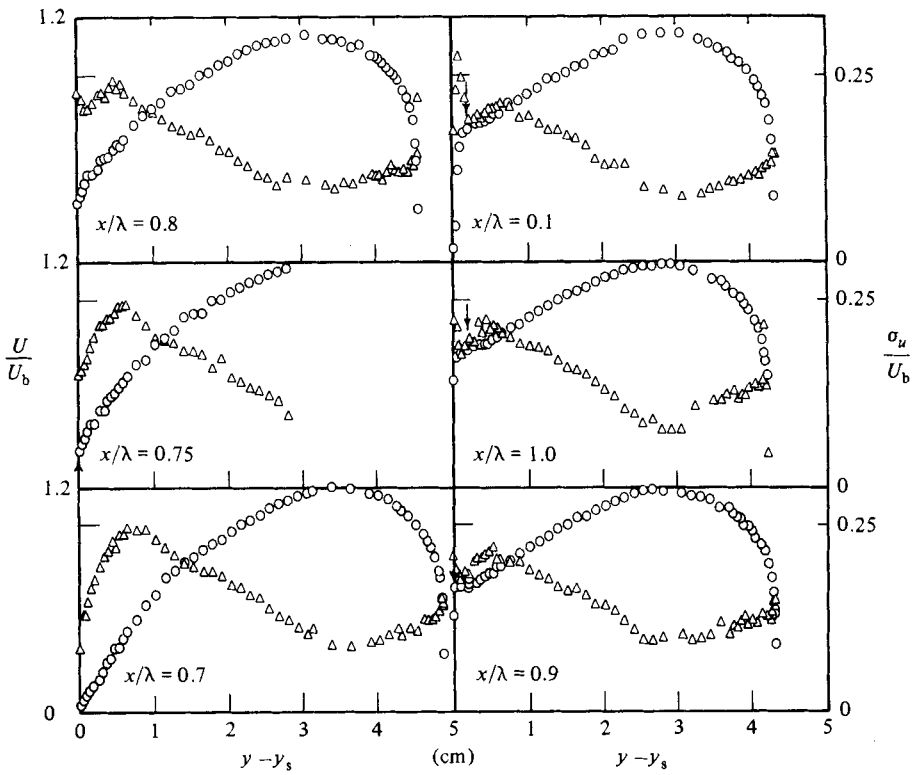

FIGURE 8. Time-averaged velocity and turbulent intensity for $x/\lambda = 0.7$ to 0.1. ○, U/U_b; △, σ_u/U_b.

attachment point, as evidenced by the sharp change of the velocity close to the wall from $x/\lambda = 0.7$ to $x/\lambda = 0.6$.

Estimates of the wall shear stress τ_w, obtained by assuming a linear variation of the velocity from the wall to the first point at $y - y_s = 0.13$ mm, are plotted in figure 10. These show a sharp increase in τ_w after reattachment and a maximum at $x/\lambda = 0.85$. The thickening of the boundary layer causes a decrease in τ_w from $x/\lambda = 0.85$ to the crest, and the unfavourable pressure gradient downstream of the crest causes this decrease to become much sharper from $x/\lambda = 0$ to $x/\lambda = 0.1$. Zilker (1976) has obtained measurements of the wall shear stress using electrochemical wall probes. However, the large fluctuations of the wall shear stress around the mean, evidenced in this research, would indicate that these measurements are unreliable except near the maximum in τ_w. It is of interest that Zilker also reported this maximum to occur at $x/\lambda = 0.85$, but with a magnitude that is about 30% larger than what was measured with the LDV.

The dominant feature of the mean-velocity profiles at values of x/λ that include a separated flow is the existence of a region of high vorticity (as evidenced by large values of $\mathrm{d}u/\mathrm{d}y$) away from the surface, suggestive of a free shear layer which was formed when the boundary layer separated from the surface. The outer edge of the boundary layer is evidenced by a shoulder in profiles of mean velocity, indicated by the arrows in figures 8 and 9.

The outer shoulders in the separated profiles are clearly indicated for $x/\lambda = 0.2$, 0.3 and 0.4, and are faintly indicated for $x/\lambda = 0.5$, 0.6 and 0.7. If the boundary

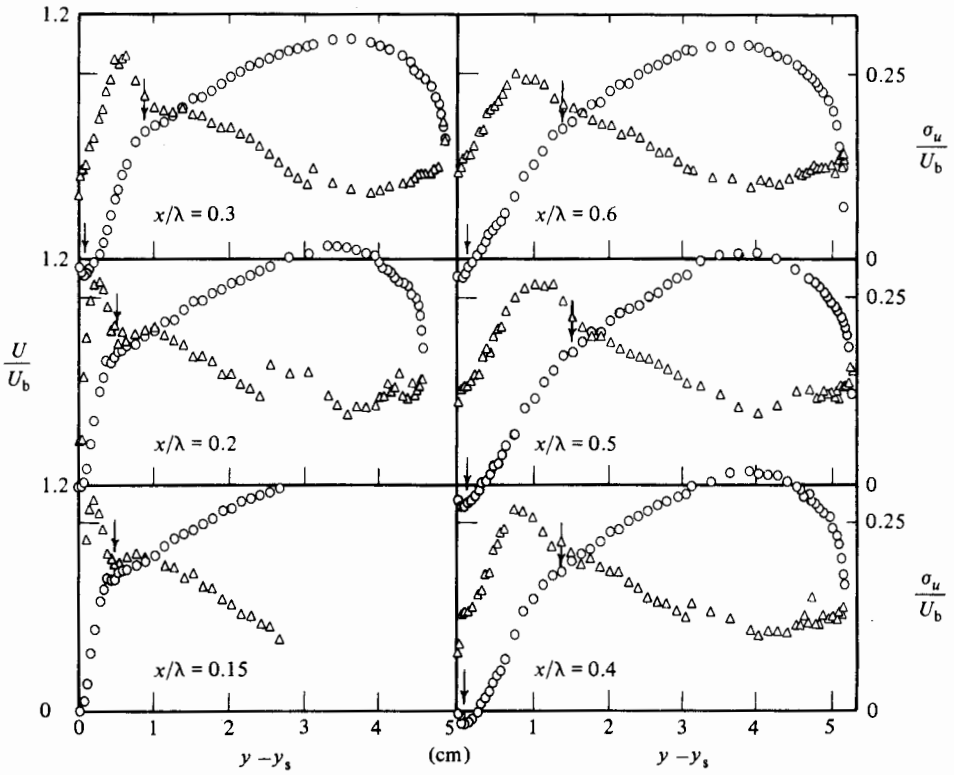

FIGURE 9. Time-averaged velocity and turbulent intensity for $x/\lambda = 0.15$ to 0.6: ○, U/U_b; △, σ_u/U_b

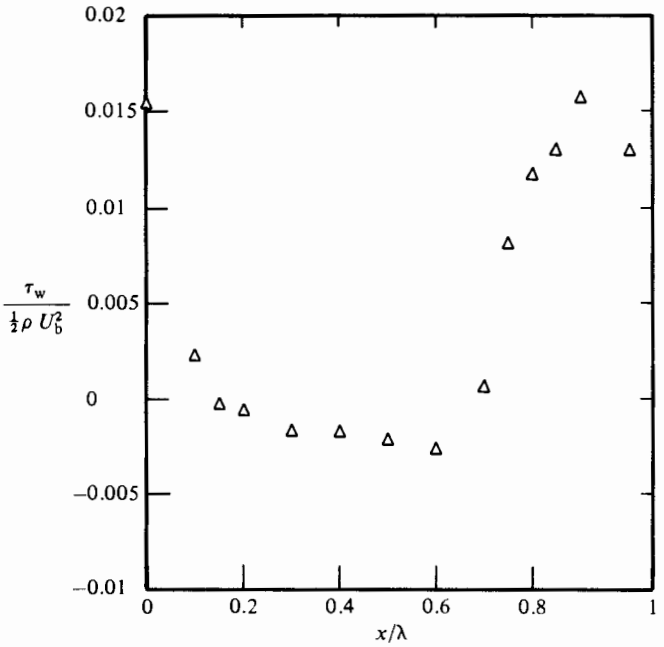

FIGURE 10. Wall-shear-stress distribution.

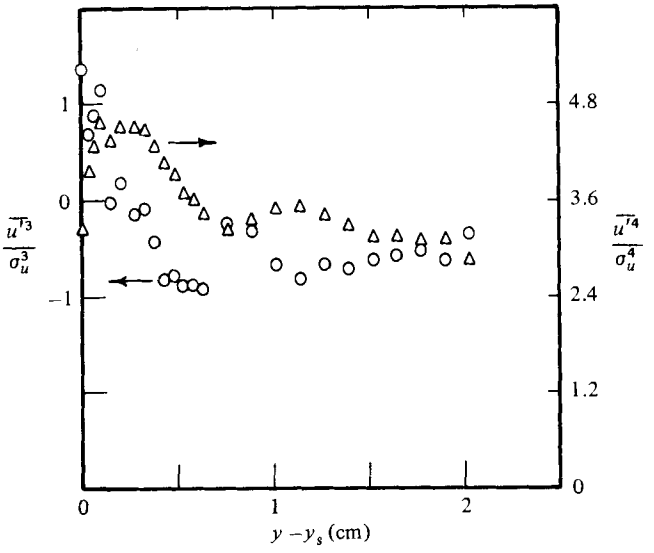

FIGURE 11. Skewness and flatness factors for $x/\lambda = 0.3$: △, skewness S; ○, flatness F.

of the free shear layer is assumed to extend out to these shoulders its change in thickness δ_{SL} in the flow direction is estimated to be

$$\frac{d\delta_{SL}}{dx} \approx 0.56 \tag{7}$$

up to $x/\lambda = 0.50$. The very large growth rate of this region reflects the large magnitude of the turbulent velocity fluctuations and the large divergence of the mean streamlines, as indicated in figure 3 from $x/\lambda = 0.15$ to $x/\lambda = 0.7$.

3.3. *Profiles of turbulence properties*

Measurements of the root-mean-square velocity fluctuations σ_u are plotted in figures 8 and 9 so that a direct comparison may be made with the profiles of mean velocity.

Downstream of reattachment ($x/\lambda = 0.8, 0.9$) a maximum in σ_u occurs for the point closest to the wall, indicating a value of $\sigma_u/U_b > 0.2$ within the turbulent boundary layer. The rapid thickening of the turbulent boundary layer causes this maximum in σ_u to move away from the wall (see $x/\lambda = 0.1, 0.15$).

Beyond $x/\lambda = 0.15$ the region of maximum intensity is far enough away from the wall that it is associated with the free shear layer, appearing approximately at the location of an inflection point in the mean-velocity profile (see $x/\lambda = 0.2, 0.3, 0.4, 0.5, 0.6, 0.7$). The magnitude of the intensity at this location is quite large ($0.2U_b$–$0.3U_b$). It is evident that this maximum in σ_u provides a much more sensitive means of locating the free shear layer than the average velocity profiles. Thus at $x/\lambda = 0.75, 0.8, 0.9, 1$ and 0.1 the maximum in σ_u indicates the remnants of a free shear layer above the boundary layer that is attached to the wave surface. This maximum in σ_u can be traced beyond $x/\lambda = 0.15$, where it now indicates the remnants of an old free shear layer above a new free shear layer formed from the separated boundary layer.

Profiles of the skewness S and the flatness F are shown in figure 11 for $x/\lambda = 0.3$. The large values of the flatness close to the wall reflect the intermittency of the

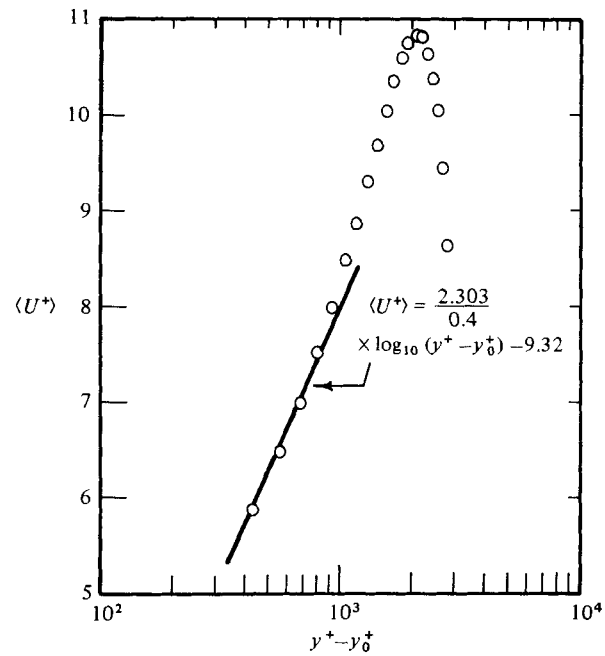

FIGURE 12. Wavelength-averaged velocity.

velocity signals in the separated region. Maximum values of around 4 occur at the location of minimum mean velocity (maximum reversed flow). Full flatness data are available in Buckles (1983). The most important feature of the skewness profile are the two zero-crossings. The skewness changes sign in the free shear layer, roughly at the maximum in the turbulent intensity or the inflexion point of the average velocity profile. The positive skewness close to the wall reflects the intermittent bursts of positive velocity indicated in the signals displayed in figure 6. The maximum value of the skewness occurs roughly at the location where the average velocity is zero.

In the immediate vicinity of the wall the skewness again changes sign, as had previously been found by Simpson *et al.* (1981*b*). This behaviour is similar to what is found at $y^+ \approx 10$ for turbulent flow over a flat plate. However, in this case the point closest to the wall has a skewness of opposite sign to what is observed for a flat plate because the fluid close to the wall is moving, on average, in the negative direction.

3.4. *Wavelength-averaged properties*

The force F_x acting on the wave per unit area in the x-direction can be calculated from the measured profiles of pressure and shear stress along the surface:

$$F_x = \int_0^1 \left[\tau_w\left(\frac{x}{\lambda}\right) - P_w\left(\frac{x}{\lambda}\right) \frac{2\pi a}{\lambda} \sin\left(\frac{2\pi x}{\lambda}\right) \right] \frac{\mathrm{d}x}{\lambda}, \tag{8}$$

where τ_w is the shear stress on the surface due to skin friction, and P_w is the measured pressure at the surface. A value of $F_x = 37.5$ dyn/cm^2 is obtained from the results shown in figures 5 and 10. The contribution from τ_w is small, being only 3.6 dyn/cm^2. A friction velocity, defined as $v^* = (F_x/\rho)^{\frac{1}{2}}$, is calculated as 6.1 cm/s.

The local velocity profiles shown in figure 8 depart dramatically from the logarithmic profile characteristic of turbulent flow over a flat plate. However, it is of interest to determine whether wavelength-averaged velocities, measured above the

wave crest, give a behaviour similar to what is observed for flow over a sand-roughened surface. These averages, calculated at a fixed distance from the trough, are plotted in figure 12 as $\langle U\rangle/v^*$ versus $(y-y_0)v^*/\nu$. The origin y_0 is taken to be the average location of the wave surface, $y = a$.

The straight line shown in figure 12 is described by the equation

$$\langle U\rangle^+ = \frac{1}{\kappa}\ln(y^+ - y_0^+) + B, \tag{9}$$

where $\kappa = 0.4$ is the von Kármán constant and $B = -9.3$. Flow over a completely roughened sand surface (Schlichting 1960) is given by an equation of the same form as (9) with

$$B = 8.5 - 2.5\ln\frac{k_s v^*}{\nu}. \tag{10}$$

A comparison of the straight-line fit to the data close to the wall in figure 12 with (9) and (10) therefore gives a value of k_s^+ of 1480, or $k_s/2a = 2.4$, characterizing the wave surface.

4. Discussion

This paper presents the first comprehensive results on the separated regions that exist for turbulent flow over large-amplitude wavy surfaces. The picture that emerges is quite different from what is found for laminar separated flows in that the region of reversed flow varies dramatically with time and nowhere in the flow field is the velocity in the reverse direction 100 % of the time. However, time-averaged streamlines can be calculated from the time-averaged velocities. These define a separated zone in which the flow is intermittently in the forward and reverse direction and give an outer boundary for the reversed flow which corresponds roughly to the location where the flow is in the forward direction 50 % of the time. The velocity signal in and near the separated region has a spiky appearance and shows excursions in time for which the change in the velocity can be several times as great as the average velocity. This is evidenced by large intensities and large flatness factors for the fluctuating velocity signal.

Separation and reattachment points are defined as locations where the time-averaged velocity gradient at the wall is zero. These agree (as suggested by Kline, Bardina & Strawn 1981) approximately with the extrapolation of the line of 50 % intermittency to the wave boundary. The separation point occurs where there is an unfavourable pressure gradient and the reattachment point occurs just upstream of the maximum in the pressure.

The reattachment point has as its signature a maximum, of large magnitude, in the root-mean-square value of the pressure fluctuations. At the reattachment point, boundary layers form along the wall in both the upstream and downstream directions. The boundary layer in the upstream direction is not well defined and could progress only a short distance. The boundary layer in the downstream direction is quite thin and turbulent, as evidenced by the existence of a maximum in the turbulent intensity within it. This boundary layer progresses to the separation point on the next wave, where it separates from the surface as a free shear layer. This shear layer spreads quite rapidly downstream of separation owing to the high intensity of the turbulence and the divergence of the mean streamlines. A maximum in the intensity of the turbulent velocity fluctuations occurs in the free shear layer, approximately at an inflexion point of the mean-velocity profile. The location of the shear layer can, in fact, be

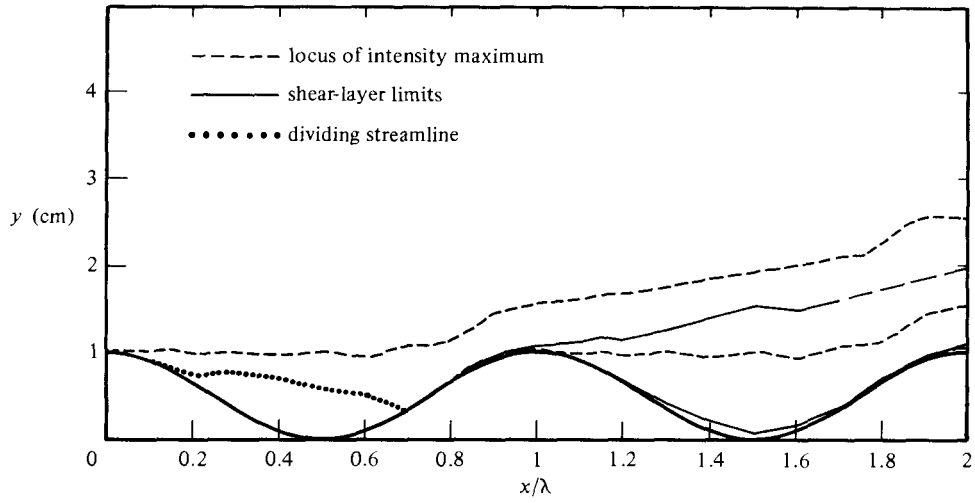

FIGURE 13. Shear-layer map.

defined more precisely through this maximum than it can through the average-velocity profile, making it possible to map the trajectory of each shear layer.

In this way we can detect the layering of the flow shown in figure 13. For example, at $x/\lambda = 2.0$ three local maxima can be discerned. One is in the attached boundary layer. The other two are from free shear layers formed by the separation of a boundary layer at $x/\lambda = 1.14$ and at $x/\lambda = 0.14$.

In a region extending approximately one-half wavelength downstream of the crest, the primary shear layer (the layer formed by the most recent separation) spreads in a nearly linear manner about a shear layer centreline that is approximately horizontal. The rate of spread, defined as the ratio of the distance between the shoulder of the shear layer and the distance along the centreline, is about 0.16 on the upper side of the layer. In comparison, a typical half-layer spread rate for a plane shear layer with zero velocity on the low-speed side is 0.18 ± 0.04. Direct comparisons of growth rates are subject to uncertainty because shear-layer growth depends upon several parameters, including the state of the initial boundary layer, freestream turbulence, and the presence of periodic perturbations which determine the initial Strouhal number of the shear layer (Weisbrot, Einav & Wygnanski 1982). However, within the limits of these uncertainties the top half of the separated shear layer in the present experiments appears to interact with the freestream in a manner that is not dissimilar to that of a plane free shear layer.

The spread rate that we observe on the bottom half of the shear layer (i.e. towards the wave trough) is approximately 0.4 in the first one-half wavelength downstream of the separation point, and is thus much larger than what is observed for the top half or for a free shear layer. The large discrepancy between this spread rate and that of a plane free shear layer shows that the separated shear layer cannot be modelled entirely as an unbounded shear layer. This conclusion is consistent with the work of Bradshaw & Wong (1972), but it contrasts with the work of Eaton & Johnston (1981), which concluded that the separated flow over a rearward-facing step quantitatively resembles an ordinary free shear layer up to a downstream location where wall-interference effects could not be neglected. This occurred at about one-half of the mean reattachment length. It appears that the separated shear layer that occurs for a rearward-facing step grows as an unbounded shear layer because it is initiated at

a distance from the lower boundary. In contrast, the shear layer in the wavy surface flow is always affected by the proximity of the boundary because the surface drops slowly away from the shear layer centreline downstream of separation.

Visualization of separated flow over a wave using surface-injected dye streaks (Zilker & Hanratty 1979) shows the separated shear layer rolling up into vortices which fill the entire wave trough. In contrast, if this region behaved as a free shear layer, we would expect instead to see more isolated eddy structures with a passive fluid in the reversed-flow zone separating the shear layer from the wave surface.

The photographs of Zilker showed columnar motions carrying dye between the wave surface and the shear layer. The directions of these flows cannot be ascertained, but the wall 'splat' effect discussed in conjunction with the present intermittency data indicates that at least some of the dye columns correspond to strong intermittent downward motions.

The data suggest a qualitative picture of the flow in which shear layer vortices send fluid downward toward the wall and entrain fluid from the reversed flow region upwards into the shear layer. Large positive skewness values and large flatness values in the reversed-flow region near the wall imply intermittent pulses of forward-moving fluid, possibly associated with the passage of shear-layer vortices overhead. We note that this picture is similar in many regards to the model proposed By Simpson *et al.* (1981*a*, *b*) for a separating turbulent boundary layer.

This work is being supported by the National Science Foundation under Grant NSF CPE 79-209804 and by Shell Oil Foundation.

REFERENCES

ABBOTT, D. E. & KLINE, S. J. 1962 *Trans. ASME* D: *J. Basic Engng* **84**, 317–325.

ADRIAN, R. J. 1983 In *Fluid Mechanics Measurements* (ed. R. J. Goldstein). Hemisphere.

BRADSHAW, P. W. & WONG, F. Y. F. 1972 *J. Fluid Mech.* **52**, 135.

BUCKLES, J. J. 1983 Turbulent separated flow over wavy surfaces. Ph.D. Thesis, Univ. Illinois, Urbana.

CAPONI, E. A., FORNBERG, B., KNIGHT, D. D., MCLEAN, J. W., SAFFMAN, P. G. & YUEN, H. C. 1982 *J. Fluid Mech.* **124**, 347.

DURST, F. & PEREIRA, J. C. F. 1982 In *Proc. Intl Symp. on Appl. Laser-Doppler Anemometry to Fluid Mechanics, Lisbon 5–7 July* (eds D. F. G. Durão, R. J. Adrian, F. Durst, H. Mishina & J. H. Whitelaw).

EATON, J. K. & JOHNSTON, J. P. 1981 *AIAA J.* **19**, 1093–1100.

ETHERIDGE, D. W. & KEMP, P. H. 1978 *J. Fluid Mech.* **86**, 545–566.

GEORGE, W. K. 1974 In *Proc. 2nd Intl Workshop on Laser Velocimetry, Purdue University, 27–29 March*, pp. 511–516. Purdue University Engineering Experiment Station.

HILLIER, R. & CHERRY, N. J. 1982 In *Turbulent Shear Flows, 3* (ed. L. J. S. Bradbury, F. Durst, B. E. Launder, F. W. Schmidt & J. H. Whitelaw). Springer.

KIM, J., KLINE, S. J. & JOHNSTON, J. P. 1978 *Thermosci. Div. Dept. Mech. Engng, Stanford Univ. Rep.* MD-37.

KLINE, S. J., BARDINA, J. & STRAWN, R. 1981 Detachment and reattachment of turbulent boundary layers on two-dimensional faired surfaces. AIAA-81-1220, *AIAA 14th Fluid and Plasma Dyn. Conf. 23–25 June, Palo Alto.*

MAYBEY, D. G. 1972 *AIAA J. Aircraft* **10**, 642–645.

REISCHMANN, M. M. & TIEDERMAN, W. G. 1975 *J. Fluid Mech.* **70**, 369–392.

ROBERTSON, J. M., WEDDING, J. B., PETERKA, J. A. & CERMAK, J. E. 1977 *J. Indust. Aerodyn.* **2**, 345–359.

SIMPSON, R. L., CHEW, Y. T. & SHIVAPRASAD, B. G. 1981*a* *J. Fluid Mech.* **113**, 23–51.

SIMPSON, R. L., CHEW, Y. T. & SHIVAPRASAD, B. G. 1981*b* *J. Fluid Mech.* **113**, 53–73.

SIMPSON, R. L., STRICKLAND, J. H. & BARR, P. W. 1977 *J. Fluid Mech.* **79**, 553–594.

SCHLICHTING, H. 1960 *Boundary Layer Theory*, 4th edn, chap. XX. McGraw-Hill.

THORSNESS, C. B. 1975 Transport phenomena associated with flow over a solid wavy surface. Ph.D. Thesis, Univ. Illinois, Urbana.

THORSNESS, C. B., MORRISROE, P. E. & HANRATTY, T. J. 1978 *Chem. Engng Sci.* **33**, 579–592.

WEISBROT, I., EINAV, S. & WYGNANSKI, I. 1982 *Phys. Fluids* **25**, 1691–1693.

ZILKER, D. P. 1976 Flow over wavy surfaces. Ph.D. Thesis, University of Illinois, Urbana.

ZILKER, D. P., COOK, G. W. & HANRATTY, T. J. 1977 *J. Fluid Mech.* **82**, 29–51.

ZILKER, D. P. & HANRATTY, T. J. 1979 *J. Fluid Mech.* **90**, 257–271.